A theoretical study of the potential energy surface for the isomerization reaction of fluoranthene to aceanthrylene: Implications for combustion chemistry

Thanh-Binh Nguyen, Dorra Khiri, Sonia Taamalli, Laurent Gasnot, Florent Louis, Abderrahman El Bakali, Duy Quang Dao

A theoretical study of the potential energy surface for the isomerization reaction of fluoranthene to aceanthrylene: Implications for combustion chemistry

Thanh-Binh Nguyen,[1] Dorra Khiri,[2] Sonia Taamalli,[2] Laurent Gasnot,[2] Florent Louis,[2]

Abderrahman El Bakali,[2,*] and Duy Quang Dao[3,4,*]

[1]*Faculty of Chemical Engineering, The University of Da Nang - University of Science and Technology, 54 Nguyen Luong Bang St., Da Nang, 550000, Viet Nam*

[2]*Université de Lille, CNRS, UMR 8522 - PC2A - PhysicoChimie des Processus de Combustion et de l'Atmosphère, 59000 Lille, France*

[3]*Institute of Research and Development, Duy Tan University, Da Nang, 550000 Viet Nam*

[4]*Faculty of Environmental and Chemical Engineering, Duy Tan University, Da Nang, 550000 Viet Nam*

Corresponding authors: daoduyquang@duytan.edu.vn (DQD)

abderrahman.el-bakali@univ-lille.fr (AEB)

ABSTRACT

Isomerization reaction of fluoranthene forming aceanthrylene was investigated using density functional theory (DFT). Geometrical structures and scaled vibrational frequencies of all species and thermodynamic properties including standard reaction enthalpies $\Delta_r H°(T)$ and Gibbs free energies $\Delta_r G°(T)$ were calculated at a wide range of temperature from 298 to 2500 K at the B97D3/6-311++G(3df,2p)//B97D3/6-311++G(d,p) level of theory. Consequently, the fluoranthene isomerization is initiated *via* two pathways, either by hydrogen 1,2-shift or carbon 1,2-shift reactions with reaction barrier of 356.6 and 393.6 kJ mol^{-1}. Also, the co-existence of aceanthrylene and acephenanthrylene was observed with the corresponding $\Delta_r H°(0\ K)$ of 28.5 and 53.7 kJ mol^{-1}. Kinetic calculations for the initiative step confirm that in comparison with the carbon 1,2-shift mechanism the hydrogen 1,2-shift mechanism is always predominant. However, as shown by the kinetic calculations, these reactions are not relevant under flame conditions. It may need to find other reaction pathways explaining the conversion of these two intermediate species to pyrene.

KEYWORDS: *Isomerization, PAHs, Potential energy surface, Reaction mechanisms, Kinetic calculations.*

1. Introduction

There has been a growing need for better understanding of mechanisms of combustion processes that are driven not only by the demand to further improve the utilization of fossil energy resources, but also to control the dispersal of pollutants into the environment. Controlling the dispersal of soot particles into the air has received considerable attention, especially in the context of an increasing consumption of diesel-fueled engines in many industrial sectors and transportation vehicles. Exposure to soot particles can cause various human health-related problems such as heart diseases and lung cancer [1–4]. In addition to serious health risks, the soot deposition on surfaces of combustion chamber walls is closely associated with the emission of environmental pollutants as well as diesel-powered motor performance [5,6]. Therefore, a good knowledge of the characteristics of soot particulates and mechanisms leading to their formation is of great importance in mitigating the emission of these dangerous particles. In recent years, numerous research projects have focused on analyzing the mechanism of soot particle formation [7–13]. Yet this reaction is only partially understood.

As being widely accepted, soot particles are mainly produced from incomplete and inefficient combustion process of carbonaceous fuels (petroleum, biofuels, *etc.*) in internal combustion engines and industrial devices. The formation of these particles generally follows three consecutive (and partially parallel) steps including nucleation, surface growth and agglomeration [7]. The first step, named the nucleation process or particle inception, is considered crucial to understanding soot formation mechanisms. Numerous experimental and theoretical evidence has been reported in literature to describe the soot nucleation that commonly takes account of multi-benzene ring species, called Polycyclic Aromatic Hydrocarbons (PAHs), as precursors responsible for this step [12,14]. These precursors, which are generated from combustion process

under high temperature, will react with each other to form soot particles of larger molecular weight. A number of PAHs species along with their characteristic properties have been identified and reported in the literature [4]. It should be stressed at this point that most studies aiming at elucidating the forming mechanism of soot nucleation are focused on four ring aromatics [15–20], which are reasoned to be thermodynamically stable as compared to the two- or three-ring aromatics [21]. In addition to the reason above mentioned, considering the cancerogenic and mutagenic potentials [22], our attention in this work will be paid to fluoranthene, acephenanthrylene and aceanthrylene.

Discussion on possible mechanisms that could lead to the formation of the precursors of PAHs is thoroughly given by many researchers. It is noteworthy that although the proposed models are either experimentally or theoretically demonstrated to be useful in modeling soot formation, their accuracy varies considerably depending on combustion conditions, particularly on fuel structure (*i.e.* aromatic fuels, aliphatic fuels …). It is widely accepted that the mechanism of PAHs formation and growth goes through free radical intermediates and small aromatic rings as precursors of PAHs. One of such mechanisms is the Hydrogen Abstraction C_2H_2 Addition (HACA) mechanism, firstly proposed by Frenklach *et al.* [23] and later modified by Appel and co-workers [24]. Within this HACA framework, C_2H_2 molecules serve as building blocks in order to form initial aromatic rings and as bridge to recombine two or more small PAHs species. In contrast, Miller and Melius [25] suggested that first aromatic rings could be formed by a recombination reaction of two propargyl radicals (C_3H_3) for benzene, or between two cyclopentadienyl radicals (C_5H_5) for naphthalene. The addition mechanism of vinylacetylene (C_4H_4) into PAH radicals has also attracted attention because of the abundance of C_4H_4 in combustion environments [26,27].

Many research groups have placed their attention to the inter-conversion of a (non-)benzenoid compound into another one under the effect of heat. Discussion on the thermal rearrangement (or isomerization) mechanism, which results in the formation of aromatic species, is firstly reported by Hopf and Musso [28] and Brown *et al.* [29]. Much more related to the field of PAHs, the isomerization mechanism of aromatic compounds is originally recognized in a series of publications given by Scott *et al.* [30–33]. In these original works, the isomerization mechanism, which is generalized by observing the thermal rearrangement of azulene, naphthalene, benzene, anthracene, and pyrene involves a carbon 1,2-shift (also known as benzene ring contraction) and a hydrogen 1,2-shift, both across the same carbon–carbon bond but in opposite directions [32]. The formation of PAHs precursors *via* this mechanism has been successfully elucidated in various applications, both experimental studies and theoretical computations [33–40]. In addition, the inter-conversion between three or four ring aromatics including aceanthrylene, acephenanthrylene, and fluoranthene at high temperature was first studied by Scott *et al.* [33] Considering the experimental evidence, Scott *et al.* [33] proposed the mechanisms of forming fluoranthene from aceanthrylene through intermediate species, that is, acephenanthrylene. The conversion of acephenanthrylene into fluoranthene was also observed by Sarobe *et al.*[36] through the synthesis of cyclopenta-fused PAHs. In contrast to the results reported by Scott *et al.* [33], Sarobe *et al.* reported that there is no trace amount of aceanthrylene from the thermal conversion of acephenanthrylene. These observations are also corroborated by semi-empirical computations used by Sarobe *et al.* [36]. The inter-conversion of these three aromatic molecules under the effect of temperature has not been yet studied in the literature using either computational chemistry tools or experimental works.

Recently, by taking into consideration the isomerization process of fluoranthene to pyrene and aceanthrylene to fluoranthene, Desgroux and co-workers [40] showed a reasonably better result on modeling the soot nucleation in a “nucleation” and a “sooting” low pressure premixed methane flame. In fact, the authors showed that both peak mole fractions of fluoranthene and pyrene measured in premixed methane flames at low-pressure and atmospheric pressure are reached at the end of flame front and they are formed again in the sooting zone after a slight depletion [40]. Moreover, reactions with high activation energy play a major role in the accumulation of these two gaseous species in this specific zone. This observation was also highlighted in the case of benzene by El Bakali *et al.* [41]. It was demonstrated that the reaction of H-atom elimination from benzene, which is highly endothermic reaction (energy activation being about 380 kJ mol^{-1}) was responsible for benzene accumulation in the soot zone [41]. Moreover, a lot of HACA mechanism effectiveness were also observed and seem to be likely from a certain size of PAHs, i.e. 4- and 5-PAHs rings. The authors thus suggested that isomerization reactions contribute to the HACA mechanism breakdown due to their slowness and then contribute significantly to pyrene (and its isomer) recycling in the soot zone. This element can promote formation of the dimers of these species. Indeed, while the literature reports that only very large dimers were possible, only 4- and 5-rings dimers could experimentally be identified just before the appearance of soot particles in laminar diffusion flames [42]. These new developments are very important in development of soot codes. The coupling of the reaction gas phase mechanisms with soot programs led to the total consumption of pyrene mole fraction largely used as a direct soot nucleation process. This observation completely contradicts the experimental fact because pyrene and its isomers accumulate in the soot zone.

These important results have brought us to consensus that the formation of PAHs precursors, *e.g.* fluoranthene, in flame conditions may contribute into a better understanding of the soot nucleation and growth mechanism. Driven by the need to contributing into this fascinating debate on the governing reaction of forming fluoranthene, the objective of this paper aims at *(1)* re-investigating the thermal isomerization mechanism of converting aceanthrylene into fluoranthene *via* acephenanthrylene as an intermediate species by using theoretical computations at a high theory level, and at *(2)* providing reliably computed thermodynamic properties and kinetic parameters. The implications of the studied reactions under flame combustion conditions will be discussed.

This article is organized as follows: First, computational methods as well as the different calculation steps will be discussed in section 2. The results of two potential reaction pathways by which aceanthrylene, acephenanthrylene, and fluoranthene could be interconverted under high temperature conditions, as well as thermodynamic properties and kinetic parameters for the forward and reverse reactions in flame conditions are presented and discussed in section 3. Finally, some conclusions and perspectives are provided.

2. Methodology

All calculations were performed using Gaussian 16, Revision A.03 package [43]. Several DFT methods were evaluated such as hybrid functional B3LYP [44,45] and M06-2X [46], exchange-correlation functional BMK [47], pure functional, B97, with the Grimme's D3BJ dispersion (B97D3) [48,49], as well as composite method CBS-QB3 [50]. As a result, the B97D3 functional are the most suitable one for the studied molecular system, whereas, the other computational methods result in the problem in which the energy of product is higher than the one of TS.

Moreover, the MP2/CBS(d,t) computational scheme proposed by Varandas and co-workers[51–54] which is based on the extrapolation of MP2 calculation from cc-pVDZ and cc-pVTZ basis sets to the complete basis set (CBS) limit using a specific formalism, was also tested because it was validated for several data sets of hydrogen atom transfer and isomerization reactions. Unfortunately, the TSs of the hydrogen 1,2-shift reaction are unsuccessfully located by this approach. All the detailed information are presented in the Table S1a and S1b (SI file).

Geometrical properties of all species involved in the isomerization reaction were optimized in their electronic ground state using the pure dispersion corrected functional B97D3 [48,49] combined with the 6-311++G(d,p) basis set. The DFT approach has been recommended for kinetic calculations of hydrocarbon systems with an uncertainty of less than 2 kcal mol^{-1} for barriers [47,55–57] within an acceptable computational cost. The vibrational frequencies and zero-point energy (ZPE) of all species were scaled by a factor of 0.988 which is determined based on the comparison between the computed harmonic frequencies with the experimental ones of fluoranthene, pyrene, benzene, and naphthalene (Tables S2a and S2b in the supplementary material). The accuracy of single-point energy calculations was then improved by using a larger basis set including more polarization functions on H and C atoms, 6-311++G(3df,2p). The thermodynamic properties, *i.e.* standard reaction enthalpies $\Delta_r H°(T)$ and Gibbs free energies $\Delta_r G°(T)$, were calculated over a wide range of temperature from 298 to 1500 K. The reaction enthalpies of all studied species at different temperatures were calculated taking into account the scaled ZPE and thermal correction to enthalpy at temperature T [dd*H(T)*], which were obtained using the THERMO code [58]. Two isomerization reaction pathways were identified and the corresponding potential energy surfaces (PES) were established by characterizing all transition states (TS) and intermediate products (PRO) in which TS and local minima were checked by the

number of imaginary frequencies of 1 and 0, respectively. Furthermore, intrinsic reaction coordinates (IRC) [59] were also investigated to confirm a real connection between TS and reactant intermediate as well as between TS and product one. The stability of wave function was checked for all studied species and the geometry parameters and vibrational frequencies were calculated with a stabilized wave function using the algorithm implemented [60,61] in the Gaussian software.

Finally, the master equation calculations were performed using the MESS code [62,63] to calculate pressure- and temperature-dependent rate coefficients for both studied pathways. The Eckart barriers were used to approximate the tunneling corrections at the microcanonical level. The Lennard-Jones parameters for the studied $C_{16}H_{10}$ species (FLTHN) were used as σ = 7.17 Å and ε = 812.3 K [64]. We used argon as a bath gas which is characterized by σ = 3.462 Å and ε = 127.57 K [65].

3. Results and discussion

3.1. Structural properties and vibrational frequencies of fluoranthene, acephenanthrylene and aceanthrylene

Recently, some interesting experimental investigations have confirmed the presence of all the four species including fluoranthene, acephenanthrylene, aceanthrylene and pyrene in flame conditions. For example, Mercier *et al.* [66] reported the evolution of fluoranthene formed in a low-pressure methane sooting flame using the double imaging Photoelectron Photoion Coincidence Spectroscopy method. Furthermore, Mitra *et al.* [67] observed on the basis of the GC/MS online measurements in the atmospheric pressure laminar co-flow diffusion flame burner that the acephenanthrylene and aceanthrylene co-exist with fluoranthene and pyrene in the sooting region (from 2.5 to 3.5 cm above the burner) of the n-dodecane flame (the temperature of

flame is from 1300 to 1600K), and in the sooting region (from 1.5 to 2.5 cm above the burner) of the 1,2,4-trimethylbenzene flame (the temperature of flame is from 1300 to 1500K). The latter suggests that it may exist a thermal conversion between fluoranthene and pyrene via two intermediates being acephenanthrylene and aceanthrylene.

The conversion reaction of fluoranthene to aceanthrylene could take place *via* two possible pathways which were proposed by Scott and Roelofs [33] on the basis of their experimental observations. Scheme 1 re-sketches these two possible channels of forming aceanthrylene (PRO4) from fluoranthene (FLTHN), which were described in the original publication [33]. As shown in Scheme 1, the conversion of fluoranthene into aceanthrylene passes through an intermediate species of thermal rearrangement reactions, namely acephenanthrylene (PRO2). The hydrogen and carbon 1,2-shift mechanisms are supposed to be responsible for the thermal isomerization of all intermediate products which are formed through either the pathway (a) or (b) depends on associated reaction energies.

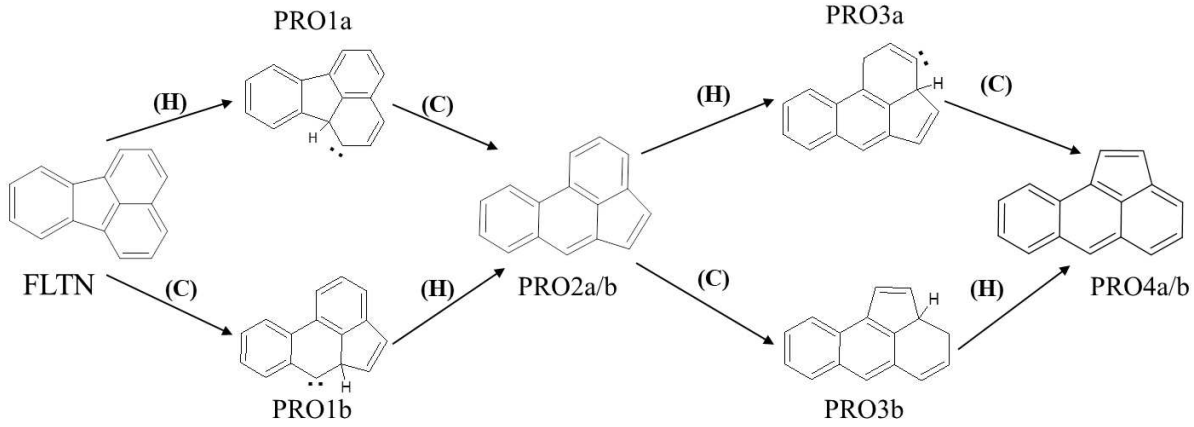

Scheme 1. Schematic presentation of fluoranthene (FLTHN) isomerization to aceanthrylene (PRO4) through acephenanthrylene (PRO2) as suggested by Scott and Roelofs in reference [33].

It is noteworthy that the proofs on the thermal isomerization mechanism for the inter-conversion among FLTHN, PRO2, and PRO4 were revised by Sarobe *et al.* [36] by means of both experimental and quantum computation approaches. However, the latter was limited only to semi-empirical AM1 level of theory for the PES calculations. Fig. 1 shows the structures of these molecules optimized at the B97D3/6-311++G(d,p) level of theory.

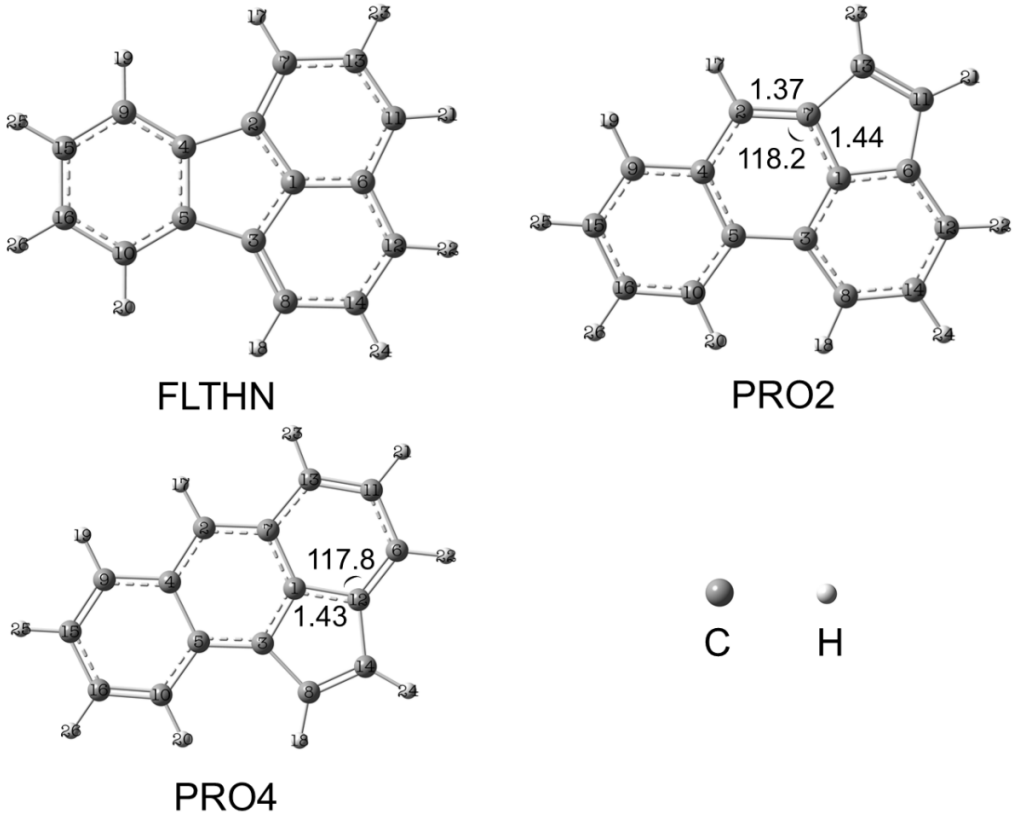

Fig. 1. Structural of fluoranthene (FLTHN), acephenanthrylene (PRO2), and aceanthrylene (PRO4) optimized at the B97D3/6-311++G(d,p) level of theory. Bond length is in Å and angle is in degree.

The comparison of the computed structural features of these three molecules with experimental and computed data available in literature is summarized in Table S3 (Supplementary Information). The bond values of these three molecules computed in this work are in a good agreement with those experimentally measured [68] as well as the values calculated [69–71] by different research groups. The optimized Cartesian coordinates at the B97D3/6-311++G(d,p) level of theory of FLTHN, PRO2 and PRO4 are summarized in Table S4 of the supplementary material.

Table 1 presents the symmetry number, electronic state, rotational constants and scaled zero-point energy (ZPE) of fluoranthene, acephenanthrylene, and aceanthrylene calculated at the B97D3/6-311++G(d,p) level of theory. At their electronic ground state, all three species display completely planar structures with the C_{2v} symmetry for fluoranthene and the C_1 symmetry for both acephenanthrylene and aceanthrylene. The unscaled vibrational frequencies of fluoranthene to be compared with the literature data are listed in Table S5 (Supplementary Information). It is observed that our results are in good agreement with the calculated ones reported by Sinha *et al.* [70] with the average deviation of 2 %.

Table 1. Symmetry number, electronic state, rotational constants, and scaled zero-point energy at the B97D3/6-311++G(d,p) level of theory for fluoranthene, acephenanthrylene, and aceanthrylene.

Species	Symmetry number	Electronic state	Rotational constants (GHz)	Scaled ZPE (kJ mol^{-1})
Fluoranthene	2	C_{2v} - $^1A_1$	1.03, 0.49, 0.33	522.3
Acephenanthrylene	1	C_1 - ^1A	1.13, 0.46, 0.33	521.4
Aceanthrylene	1	C_1 - ^1A	1.23, 0.44, 0.32	520.6

3.2. Thermo-chemical properties of fluoranthene, aceanthrylene, and acephenanthrylene

Table 2 resumes the standard molar entropy S^{o}_{298K} and the heat capacity at constant pressure $C_p^{o}(T)$ for the fluoranthene (FLTHN), acephenanthrylene (PRO2), and aceanthrylene (PRO4) calculated at the B97D3/6-311++G(d,p) level of theory. A wide range of temperature from 300 to 1500 K which corresponds to the conditions of the combustion processes was chosen to evaluate the heat capacity $C_p^{o}(T)$.

Table 2. Standard molar entropy at 298 K and constant pressure heat capacity (in J mol^{-1} K^{-1}) for fluoranthene (FLTHN), acephenanthrylene (PRO2), and aceanthrylene (PRO4) calculated at the B97D3/6-311++G(d,p) level of theory.

Species	S^{o}_{298K}	C_p^{o} (T), (J mol^{-1} K^{-1})								
	(J mol^{-1} K^{-1})	300 K	400 K	500 K	600 K	700 K	800 K	900 K	1000 K	1500 K
FLTHN	417.2	206.78	277.61	335.95	382.09	418.63	448.03	472.06	491.98	553.81
	420.5[c]/ 414.6[d]	*204.95[a] / 208.95[b]*	*274.78[a]*	*332.96[a]*	*379.38[a]*	*416.36[a]*	*446.20[a]*	*470.63[a]*	*490.88[a]*	*553.54[a]*
PRO2	423.2	207.83	278.83	337.10	383.09	419.46	448.70	472.60	492.41	553.95
	422.0[e]	*206.66[a]*	*275.92[a]*	*333.54[a]*	*379.60[a]*	*416.38[a]*	*446.11[a]*	*470.48[a]*	*490.71[a]*	*553.40[a]*
PRO4	423.86	208.56	279.50	337.68	383.58	419.88	449.06	472.90	492.67	554.10
	-	*204.34[a]*	*273.70[a]*	*331.60[a]*	*377.97[a]*	*415.01[a]*	*444.95[a]*	*469.51[a]*	*489.88[a]*	*552.98[a]*

[a]Experimental data from reference [72]; [b]Estimated data by group additivity method proposed by Pope [73]; [c]Calculated data by Bond-Centered Group Additivity of Yu *et al.* 2004 [74],[d]Calculated data of Yu *et al.* 2004 at the B3LYP/6-31G(d) level of theory [74];[e]Estimated at the B3LYP/6-311++G(d,p) level of theory by Blanquart and Pitsch [75].

As can be seen in Table 2, the data calculated in this work for FLTHN are in a good agreement with the experimental and computed ones available in literature. The calculated S^{o}_{298K} value of 417.2 J mol^{-1} K^{-1} in this work is coherent with the B3LYP/6-31G(d)-based value (414.6 J mol^{-1} K^{-1}) given by Yu *et al.* [74], with a small difference of 2.6 J mol^{-1} K^{-1}. Similarly, the difference of

the C_p^o values as compared to the experimental ones obtained by Dorofeeva *et al.* [72] varies from 0.27 at 1500 K to 2.99 J mol^{-1} K^{-1} at 500 K. The S^o_{298K} value for acephenanthrylene (PRO2) (423.2 J mol^{-1} K^{-1}) is also close to the one estimated by Blanquart and Pitsch [75] (422.0 J mol^{-1} K^{-1}). In addition, the C_p^o values obtained in this work slightly deviate from the experimental ones [72], with the deviation ranging from 0.55 to 3.56 J mol^{-1} K^{-1}. The larger deviation between the computed *vs.* experimental C_p^o values is observed in the case of PRO4 ranging from 1.12 to 6.08 J mol^{-1} K^{-1}. Table 3 presents the standard reaction enthalpies ($\Delta_r H^o$) and the Gibbs free reaction energies ($\Delta_r G^o$) computed at the B97D3/6-311++G(3df,2p)//B97D3/6-311++G(d,p) level of theory for both reactions FLTHN = PRO2 and FLTHN = PRO4.

Table 3. Standard reaction enthalpies ($\Delta_r H^o$) and standard Gibbs free reaction energies ($\Delta_r G^o$) (in kJ mol^{-1}) calculated at the B97D3/6-311++G(3df,2p)//B97D3/6-311++G(d,p) level of theory.

Thermodynamic properties (kJ mol^{-1})	Temperature (K)	FLTHN = PRO2		FLTHN = PRO4	
		This work	Literature	This work	Literature
$\Delta_r H^o$	298	28.6	30.8[a]/ 34.0[b]	53.9	61.7[b] / 53.7[c]
	1500	29.3	34.0	55.1	61.7[b]
$\Delta_r G^o$	298	26.8	-	51.9	-
	1500	18.4	-	42.2	-

Note: [a] Calculated data from Blanquart and Pitsch at the B3LYP/6-311++G(d,p) level of theory [76]; [b]Calculated data at the G3MP2//B3 method from Allison and Burgess Jr. [77]; [c] Calculated data obtained at the G4MP2 method by Rayne and Forest [78].

The calculated $\Delta_r H^o$ values at the B97D3/6-311++G(3df,2p)//B97D3/6-311++G(d,p) level of theory slightly depend upon temperature. For instance, the $\Delta_r H^o$ values increase from 28.6 to 29.3 kJ mol^{-1} and from 53.9 to 55.1 kJ mol^{-1} for the FLTHN = PRO2 and FLTHN = PRO4 reactions, respectively. On the contrary, the $\Delta_r G^o$ values remarkably decrease from 26.8 to 18.4 kJ mol^{-1} for

the FLTHN = PRO2 reaction and 51.9 to 42.2 kJ mol^{-1} for the FLTHN = PRO4 reaction. In this work, the $\Delta_r H^o$ values are in a good agreement with the corresponding values reported in literature. For instance, the $\Delta_r H^o$ value at 298 K of the FLTHN = PRO2 reaction is equal to 28.6 kJ mol^{-1}, which is 2.2 kJ mol^{-1} lower than the one obtained by Blanquart and Pitsch [76] (30.8 kJ mol^{-1}). Concerning the FLTHN = PRO4 reaction, the calculated $\Delta_r H^o$ at 298 K corresponds to 53.9 kJ mol^{-1} which is in an excellent agreement with the value given by Rayne and Forest [78] (53.1 kJ mol^{-1}). The standard reaction enthalpies ($\Delta_r H^o$) and the standard Gibbs free reaction energies ($\Delta_r G^o$) of the FLTHN = PRO2 and FLTHN = PRO4 reactions at 500, 1500, and 2500 K are summarized in Table S6. In the following sections, a full discussion on the energetic diagrams of reactions involving the formation of aceanthrylene from fluoranthene will be provided at the B97D3/6-311++G(3df,2p)//B97D3/6-311++G(d,p) level of theory.

3.2. Reaction mechanisms of aceanthrylene formation from fluoranthene

3.2.1. Pathway (a)

Fig. 2 presents the energetic diagram at 0 K corresponding to the singlet PES of the pathway (a) that is characterized by four transition states (*i.e.* TS1a, TS2a, TS3a, and TS4a), three intermediate species (*i.e.* PRO1a, PRO2, and PRO3a) and two reactants (*i.e.* FLTHN and PRO4). Single-point energies were calculated at the B97D3/6-311++G(3df,2p)//B97D3/6-311++G(d,p) level of theory.

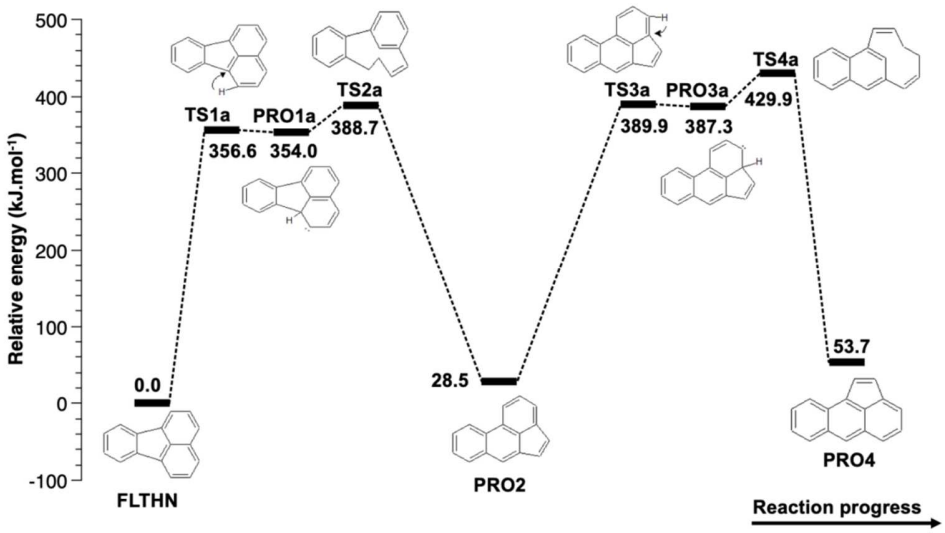

Fig. 2. Potential energy surface at 0 K for the pathway (a) of the formation of aceanthrylene from fluoranthene computed at the B97D3/6-311++G(3df,2p)//B97D3/6-311++G(d,p) level of theory.

The B97D3/6-311++G(d,p) optimized structures of the transition states, intermediates, and reactants involved in the pathway (a) are summarized in Fig. 3. The optimized Cartesian coordinates and scaled vibrational frequencies of all species appeared in the pathway (a) are given in the Table S7.

It can be seen in the reaction energy diagram (Fig. 2) that the FLTHN-to-PRO4 conversion is a multi-step process. Firstly, the pathway (a) occurs with the hydrogen 1,2-shift reaction resulting in the formation of PRO1a. By this reaction, the hydrogen atom H17, which is attached to C7 was transferred to C2 carbon atom (see Fig. 3). Several key geometrical parameters of PRO1a were modified, that is, *(i)* the C7–H17 bond length increased up to 1.98 Å as compared to 1.46 Å in TS1a, *(ii)* the dihedral angle formed by C9C4C2H17 slightly increased in comparison with the initial values of TS1a, from 61.3 to 73.1°. The transition state of this step, *i.e.* TS1a, is characterized by an imaginary frequency of 708*i* cm^{-1}, an elongation of the C7–H17 bond length

to 1.46 Å compared to the initial value of 1.09 Å in FLTHN and by a relative enthalpy of 356.6 kJ mol^{-1} compared to FLTHN. The reaction proceeds further with two parallel processes: (1) lengthening and breaking the C1–C2 bond and (2) shifting C7 carbon atom into C1 atom to form the new C1–C7 bond. As a result, the five-membered ring of PRO1a is transformed into the benzyl ring and this transformation produces a new product called acephenanthrylene (PRO2) with a low relative enthalpy of 28.5 kJ mol^{-1} compared to FLTHN. This intermediate species is characterized by several geometrical parameters such as the C2–C7 and C7–C1 bond lengths of 1.37 and 1.44 Å respectively and by the angle ∠ C2-C7-C1 of 118.2° (Fig. 1). The transition state of this step, namely TS2a, with the imaginary frequency of 558*i* cm^{-1} and the relative enthalpy at 0 K of 388.7 kJ mol^{-1}, is described by some characteristic parameters including: *(i)* the C1–C2 bond length of 1.58 Å and the C1–C7 distance of 2.17 Å and *(ii)* the ∠C2-C7-C13 angle of 114.1°. The calculated relative enthalpy values of PRO2 (28.5 kJ mol^{-1}) is about 4.9 kJ mol^{-1} smaller than the value reported by using the semi-empirical AM1 method (33.4 kJ mol^{-1}). [36] The product PRO2 continues to be converted into PRO3a *via* the hydrogen 1,2-shift reaction which in demonstrated by the transfer of H22 hydrogen atom from C12 to C6 position (Fig. 3). The transition state proposed for this step, namely TS3a, is characterized by an imaginary frequency of 681*i* cm^{-1}, the C6–H22 bond length of 1.20 Å, and the C12–H22 bond length of 1.47 Å. The formation of aceanthrylene (PRO4) from PRO3a (387.3 kJ mol^{-1}) is based on the carbon 1,2-shift mechanism, which is illustrated by shifting C12 into C1 carbon atom to form a new C1–C12 bond and by breaking the C1–C6 bond in order to form a six-membered ring (see Fig. 3). Taking further consideration on structural features of PRO4, the shifting is demonstrated in the reduced value of C1–C12 distance from 2.54 (in PRO3a) to 1.43 Å. In addition, the ∠C1-C12-C6 angle is opened from 31.5 to 117.8° (Fig. 1). The transition state of this step TS4a (Fig.

3) is identified by an imaginary frequency of 632.5*i* cm^{-1} and a relative enthalpy at 0 K of 449.9 kJ mol^{-1}. The C6–C12 bond length is almost the same in both PRO3a and TS4a, except for the dihedral angle formed by C3C1C6C12 which increases from 22.9 in PRO3a to 49.1°. The relative enthalpy at 0 K of PRO4 is 53.7 kJ mol^{-1} compared to FLTHN.

Table 4 resumes the symmetry number, electronic state, rotational constants, scaled ZPE (in kJ mol^{-1}) and S^{o}_{298K} for the different species located in the pathway (a) calculated at the B97D3/6-311++G(d,p) level of theory.

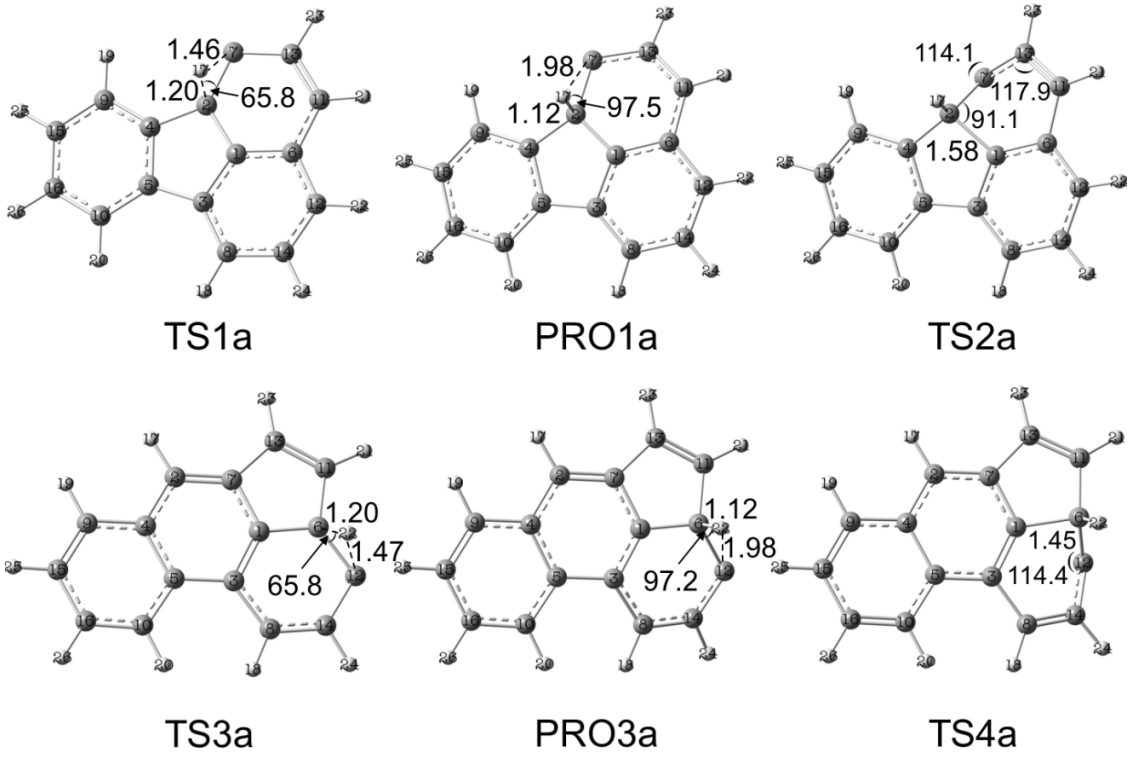

Fig. 3. Optimized structures of reactants, intermediates, products, and transition states in the reaction pathway (a) calculated at the B97D3/6-311++G(d,p) level of theory. Bond length is in Å and angle is in degree.

Table 4. Symmetry number, electronic state, rotational constants, scaled ZPE (in kJ mol^{-1}), and S^{o}_{298K} for all species involved in the pathway (a) calculated at the B97D3/6-311++G(d,p) level.

Species	Symmetry number	Electronic state	Rotational constants (GHz)	Scaled ZPE (kJ mol^{-1})	S^{o}_{298K} (J mol^{-1} K^{-1})
TS1a	1	C_1 - $^1A_1$	1.02, 0.49, 0.33	507.1	425.0
PRO1a	1	C_1 - ^1A	1.02, 0.49, 0.34	511.9	435.2
TS2a	1	C_1 - $^1A_1$	1.08, 0.48, 0.34	509.9	424.1
TS3a	1	C_1 - ^1A	1.13, 0.46. 0.33	505.9	425.4
PRO3a	1	C_1 - ^1A	1.14, 0.46, 0.33	510.3	434.6
TS4a	1	C_1 - ^1A	1.14, 0.47, 0.34	507.8	425.1

As a concluding remark, the isomerization of fluoranthene to form aceanthrylene involves two sequential processes including the hydrogen 1,2-shift and carbon 1,2-shift reactions with the reaction barrier of the initiative step being 356.6 kJ mol^{-1}. It can also be seen that the first reaction pathway is thermodynamically exothermic and non-spontaneous with all the reaction barriers being positive.

3.2.2. Pathway (b)

This section discusses the formation of PRO4 from FLTHN *via* the pathway (b), which proceeds in a similar way to the pathway (a) with consecutive hydrogen and carbon 1,2-shift mechanisms, but in a reverse order. Therefore, only the first and the last conversion will be discussed in this section. The other steps occur in a very similar way to the pathway (a).

Fig. 4 presents the reaction profile at 0 K of the pathway (b) demonstrating the conversion of FLTHN into PRO4 that is characterized by four transition states (*i.e.* TS1b, TS2b, TS3b, and TS4b), three intermediate species (*i.e.* PRO1b, PRO2, and PRO3b) and two reactants as previously discussed. It should be noted that all the single-point calculations were also obtained

by using the B97D3/6-311++G(3df,2p)//B97D3/6-311++G(d,p) level of theory. The optimized structures of these transition states, intermediates, and reactants at the B97D3/6-311++G(d,p) level of theory are summarized in Fig. 4. The optimized Cartesian coordinates and the scaled vibrational frequencies of the different species appeared in the pathway (b) are given in the Table S8 of the supplementary material.

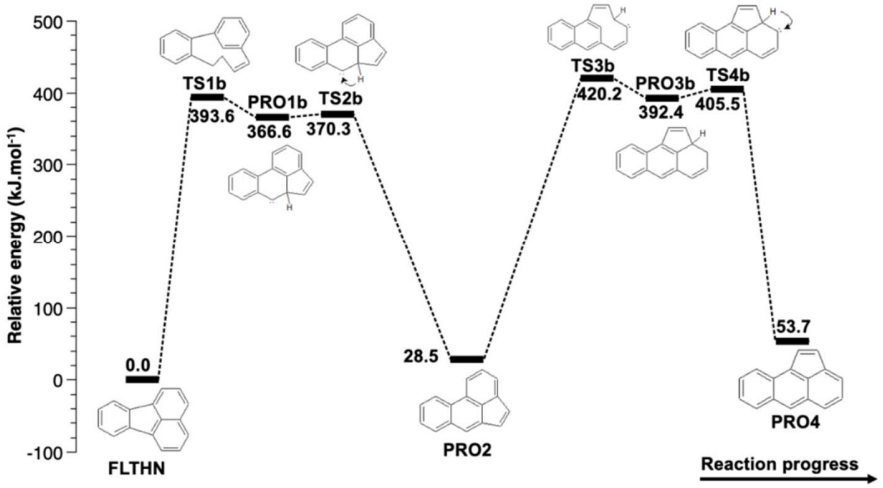

Fig. 4. Potential energy surface at 0 K for the pathway (b) of the formation of aceanthrylene from fluoranthene computed at the B97D3/6-311++G(3df,2p)//B97D3/6-311++G(d,p) level of theory.

As shown in Fig. 4, the reaction pathway (b) is initiated with the carbon 1,2-shift reaction which takes place at the C7 position in FLTHN and forms PRO1b. By this mechanism, the carbon atom from the C7 position is inserted in the five-membered ring composing of C1, C2, C3, C4, and C5 in which the C1–C2 bond is lengthened from 1.42 Å in FLTHN to 2.16 Å in TS1b, and the C1–C7 bond length is reduced from 2.40 Å in FLTHN to 1.56 Å in TS1b. The transition state of this step TS1b is identified with an imaginary frequency of 407*i* cm^{-1} and is characterized by a relative enthalpy at 0 K of 393.6 kJ mol^{-1}, which is about 37.0 kJ mol^{-1} higher

than the one of TS1a (*i.e.* 356.6 kJ mol^{-1}). The reaction pathway (b) is therefore less thermodynamically favorable than the pathway (a). This observation will be more discussed through kinetic calculations for these two initiative reactions in the last section of this work. Based on the transition state structure of TS1b, the result of an Intrinsic Reaction Coordinate (IRC) calculation confirms the formation of PRO1b (the relative enthalpy of 366.6 kJ mol^{-1}). Moreover, as shown in Fig. 5, several key structural features of PRO1b were modified including: (*i*) the angle formed by C1, C7 and C2 is increased to 118.9 compared to 91.6° in TS1b, (*ii*) the C1–C7 bond length is slightly reduced from 1.51 Å in TS1b to 1.49 Å, (*iii*) the structure of PRO1b becomes more planar based on the observation that the dihedral angle formed by ∠C1-C4-C2 surface and C7 changes from 43.0 to 11.7°.

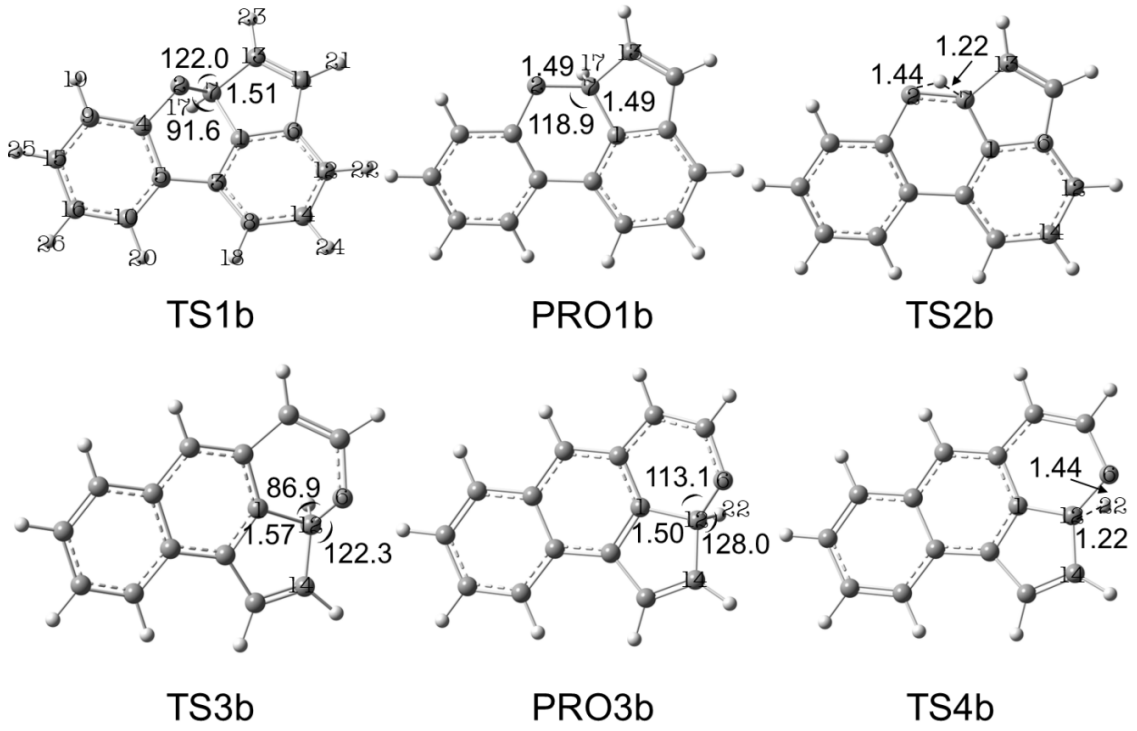

Fig. 5. Optimized structure of reactants, intermediates, products and transition states in reaction pathway (b) optimized at the B97D3/6-311++G(d,p) level of theory. Bond length is in Å and angle is in degree.

The last step in the formation of aceanthrylene (PRO4) via the pathway (b) proceeds with the hydrogen 1,2-shift mechanism, which is described by a transfer of the hydrogen atom H22 from C12 to C6 carbon atoms (Fig. 5). This procedure begins with PRO3b (392.4 kJ mol^{-1}) characterized by several key structural features such as the C1–C12 bond length of 1.50 Å and the ∠C1-C12-C6 angle of 113.1°. The transition state TS4b is determined to be necessary in the conversion of PRO3b into PRO4. The TS4b is identified by an imaginary frequency of 896i cm^{-1} and a relative enthalpy at 0 K of 405.5 kJ mol^{-1}. The symmetry number, electronic state, rotational constants, scaled ZPE and S^{o}_{298K} for the different species located in the PES of pathway (b) are resumed in Table 5.

Table 5. Symmetry number, electronic state, rotational constants, scaled ZPE (in kJ mol^{-1}), and S^{o}_{298K} for all species related to the pathway (b) calculated at the B97D3/6-311++G(3df,2p)// B97D3/6-311++G(d,p) level of theory.

Species	Symmetry number	Electronic state	Rotational constants (GHz)	Scaled ZPE (kJ mol^{-1})	S^{o}_{298K} (J mol^{-1} K^{-1})
TS1b	1	C_1 - $^1A_1$	1.14, 0.47, 0.34	510.4	423.5
PRO1b	1	C_1 - ^1A	1.12, 0.46, 0.33	512.0	431.4
TS2b	1	C_1 - $^1A_1$	1.12, 0.46, 0.33	506.2	425.3
TS3b	1	C_1 - ^1A	1.19, 0.46, 0.33	509.1	423.0
PRO3b	1	C_1 - ^1A	1.22, 0.44, 0.32	510.1	431.1
TS4b	1	C_1 - ^1A	1.23, 0.43, 0.32	504.7	426.9

As a concluding remark, the reaction pathway (b) for the fluoranthene isomerization into aceanthrylene is initiated by a carbon 1,2-shift reaction with a relative enthalpy of 393.6 kJ mol^{-1} which is thermodynamically higher than the initial reaction within the pathway (a) which begins

by a hydrogen 1,2-shift reaction a the relative enthalpy of 356.6 kJ mol^{-1}. In addition, this mechanism involves two consecutive processes of the sequential carbon 1,2-shift and hydrogen 1,2-shift reactions. It is also observed that this pathway is exothermic and non-spontaneous with all reaction enthalpies of positive values. In the final section, these two reaction pathways will be evaluated in terms of kinetics of the initiative reactions.

3.3. Kinetic parameters

The two reaction pathways (a) and (b) are respectively initiated by the FLTHN = PRO1a and FLTHN = PRO1b reactions which are thermodynamically characterized by the reaction barriers equal to 356.6 and 393.6 kJ mol^{-1}, respectively. The kinetic parameters for these reactions are computed over a wide range of temperature from 1300 – 2500 K to confirm the competition between the hydrogen 1,2-shift (pathway (a)) and carbon 1,2-shift (pathway (b)) reactions. The master equation calculations were performed with Eckart tunneling corrections as implemented in the Master Equation code MESS program [62,63]. As a result, the modified Arrhenius expressions of forward (k_f) and reverse (k_r) reactions for the reaction FLTHN = PRO1a are as follows:

k_f (in s^{-1}) = $1.06 \times 10^{13}\ T^{0.31} \exp(-43470/T)$

k_r (in s^{-1}) = $2.56 \times 10^{12}\ T^{0.11} \exp(-420/T)$

Similarly, the ones for the reaction FLTHN = PRO1b are given by

k_f (in s^{-1}) = $2.11 \times 10^{13}\ T^{0.20} \exp(-48020/T)$

k_r (in s^{-1}) = $7.16 \times 10^{12}\ T^{0.00} \exp(-3445/T)$

Table 6 resumes the forward and reverse rate constants of the initiative reactions for both studied pathways (a) and (b), respectively, over the large temperature range from 1300 – 2500 K at high pressure. It can be observed that the forward reaction of pathway (a) is always more predominant than the one of pathway (b). For example, at 1500 K the k_f value of the FLTHN = PRO1a reaction is 23 times higher than the one of the FLTHN = PRO1b reaction. Again, this observation confirms that the pathway (a) initiated by the hydrogen 1,2-shift reaction is more preponderant than the pathway (b) initiated by the carbon 1,2-shift reaction. Furthermore, the kinetic data shows that the reverse reactions from PRO1a to FLTHN are more dominant than the forward ones. For example, at 2500 K the k_r value are about 10^6 times higher than the k_f one for the reaction FLTHN = PRO1a.

Table 6. Calculated rate constants for the forward (k_f) and reverse (k_r) reactions of the first step FLTHN = PRO1a and FLTHN = PRO1b over the temperature range from 1300 – 2500 K.

T(K)	FLTHN = PRO1a		FLTHN = PRO1b	
	k_f (s^{-1})	k_r (s^{-1})	k_f (s^{-1})	k_r (s^{-1})
1300	2.89×10^{-1}	4.04×10^{12}	7.82×10^{-3}	5.11×10^{11}
1400	3.21×10^{0}	4.16×10^{12}	1.11×10^{-1}	6.18×10^{11}
1500	2.61×10^{1}	4.29×10^{12}	1.11×10^{0}	7.28×10^{11}
1600	1.62×10^{2}	4.38×10^{12}	8.29×10^{0}	8.40×10^{11}
1700	8.17×10^{2}	4.48×10^{12}	4.90×10^{1}	9.54×10^{11}
1800	3.44×10^{3}	4.58×10^{12}	2.38×10^{2}	1.07×10^{12}
1900	1.25×10^{4}	4.66×10^{12}	9.81×10^{2}	1.18×10^{12}
2000	3.98×10^{4}	4.74×10^{12}	3.51×10^{3}	1.29×10^{12}
2500	3.29×10^{6}	5.06×10^{12}	4.46×10^{5}	1.83×10^{12}

In comparison with the initiative reaction of the direct FLTHN-to-Pyrene isomerization pathway reported by Khiri *et al.* [79], the initial reactions of both the pathways (a) and (b) are more preponderant in terms of kinetics with higher rate constants. For example, at the temperature of 1500 K the rate constant of the forward reaction k_f for the first step of FLTHN = Pyrene pathway is equal to 1.52×10^{-1} s^{-1} while the k_f value of FLTHN = PRO1a is equal to 2.61×10^{1} s^{-1} and the one of FLTHN=PRO1b being 1.11×10^{0} s^{-1}. The same observation is found for other temperatures. The current results clearly detailed in the supporting information show that for all the temperature range 1300 – 2500 K the rate constants are independent of pressure.

Reaction rate constants for each step of both studied pathways were evaluated individually via the same computational procedure. Our results correspond to the TST calculations. The different parameters of the modified Arrhenius expressions of forward (k_f) and reverse (k_r) reactions for the different sub systems are given in Table 7.

Table 7. Calculated Arrhenius parameters for the forward and reverse reactions of both studied pathways

	Forward			Reverse		
	A	n	E_a	A	n	E_a
Pathway (a)						
PRO1a = PRO2	4.80×10^{12}	0.02	36.3	8.93×10^{11}	0.21	365.1
PRO2 = PRO3a	1.10×10^{13}	0.23	367.7	5.92×10^{12}	0.02	4.6
PRO3a = PRO4	5.47×10^{12}	0.03	44.3	9.67×10^{12}	0.23	381.8
Pathway (b)						
PROb = PRO2	4.01×10^{12}	0.12	5.1	5.31×10^{12}	0.63	346.5
PRO2 = PRO3b	9.38×10^{12}	0.20	397.5	7.02×10^{12}	0.00	29.3
PRO3b = PRO4	4.22×10^{12}	0.14	14.1	4.61×10^{12}	0.34	356.5

Note: [a] A in s^{-1} and E_a in kJ mol^{-1}.

The calculated rate constants for the forward (k_f) and reverse (k_r) reactions of the different steps of each reaction channel over the temperature range from 1300 – 2500 K are detailed in the Table S9 of the supplementary material. We can derive from the rate coefficients presented in Table S9 that the rate coefficients of the reverse reaction of the PRO2 = PRO3a and PRO2 = PRO3b reactions are larger than the rate coefficients of the forward ones, while for the reactions of PRO3a = PRO4 and PRO3b = PRO4 the forward rate coefficients are larger than the reverse ones over the whole temperature range from 1300 to 2500 K.

In order to shed light on the contribution of the studied isomerization reactions FLTHN=PROD4 into the overall soot formation, we computed conversion fraction of each intermediate species (FLTHN, PRO2 and PRO4) involved in the reaction scheme in Scheme 1 by beginning with different species. The results obtained at a small reaction time of 0.1 ms and in the lower temperature zone from 1500 – 2000 K characterizing for the nucleation conditions are displayed in Fig. 6.

As a result, it is noteworthy that the contribution of the studied isomerization reactions at the nucleation conditions is observed to be very small and the title reaction is not fast enough to contribute significantly to the nucleation of soot. In such conditions, radical pathways achieving such (or similar) transformations should be faster [21,80,81]. This observation may raise a precaution to others works in the future focusing on the soot formation mechanism via the isomerization reaction pathways. It may need further works to find other reaction pathways that allow explaining the conversion of these two intermediate species to pyrene.

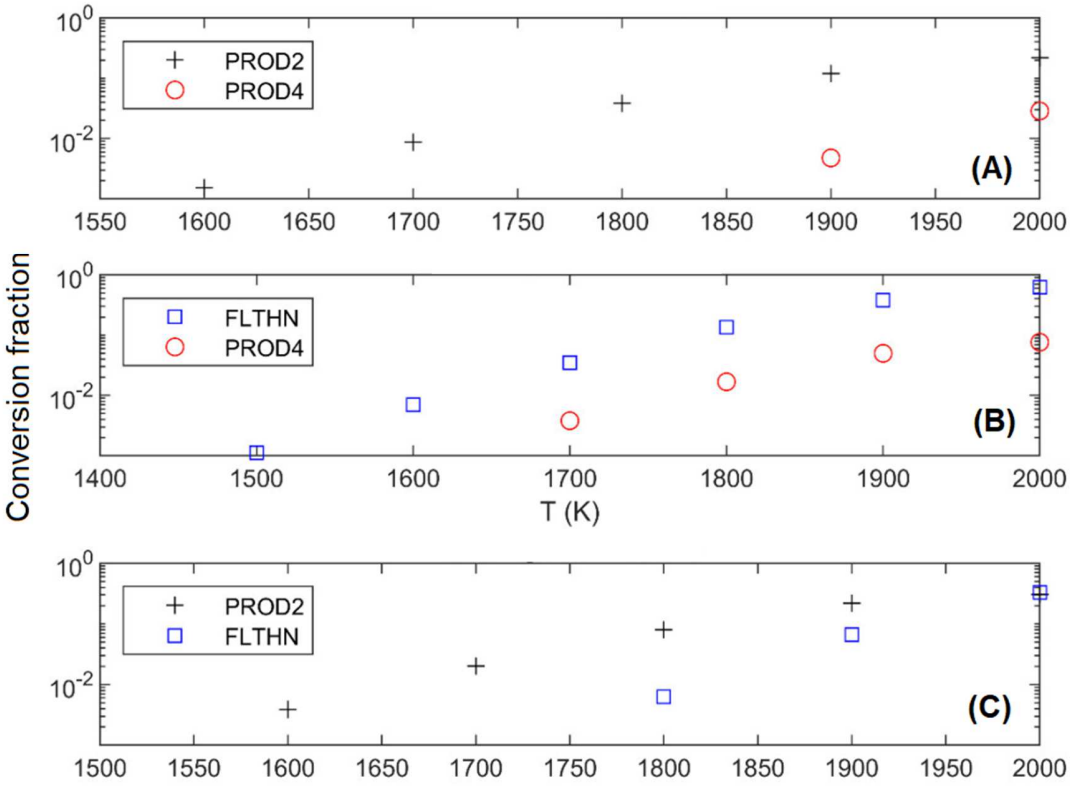

Fig. 6. Conversion fraction of three intermediate species involved in Scheme 1 (FLTHN, PRO2 and PRO4) as a function of temperature by starting with (**A**) FLTHN, (**B**) PRO2 and (**C**) PRO4. Reaction time is 0.1 ms.

4. Conclusions

The geometrical structures, electronic properties, and vibrational frequencies of fluoranthene (FLTHN) and aceanthrylene (PRO4) as well as all the intermediate species on the potential energy surface of the isomerization of FLTHN to PRO4 were investigated using density functional theory at the B97D3/6-311++G(3df,2p)//B97D3/6-311++G(d,p) level of theory. The thermochemical properties of the reactions including standard reaction enthalpies ($\Delta_r H°$) and standard Gibbs free reaction energies ($\Delta_r G°$) for all the species involving in the PES were also

calculated at a wide range of temperatures from 298 to 1500 K corresponding from the atmospheric conditions to the combustion ones. As a result, the isomerization mechanism converting fluoranthene to aceanthrylene occurs *via* two reaction pathways initiated either by hydrogen 1,2-shift (pathway a) or by carbon 1,2-shift reactions (pathway b), which are both exothermic and non-spontaneous processes. The properties showed that the pathway (a) is more favorable than the pathway (b) with the reaction enthalpies being 356.6 and 393.6 kJ mol^{-1}, respectively. Moreover, both reaction mechanisms confirm the possible co-existence of acephenanthrylene (PRO2) in flame with FLTHN and aceanthrylene (PRO4) as an important intermediate species. Indeed, the small reaction enthalpies at 0 K being 28.5 and 53.7 kJ mol^{-1} for correspondent PRO2 and PRO4 are obtained. The kinetic parameters investigated using the master equation calculations with Eckart tunneling corrections also confirmed that the pathway (a) was always more predominant than the pathway (b) with the rate constant for the forward reactions (k_f) being $1.06 \times 10^{13}\ T^{0.31} \exp(-43470/T)$ (s^{-1}) for FLTHN = PRO1a reaction and $2.11 \times 10^{13}\ T^{0.20} \exp(-48020/T)$ (s^{-1}) for FLTHN = PRO1b reaction. As discussed, these isomerization reactions are not fast enough to contribute significantly to the nucleation of soot. Thus, further works may need to explore other reaction pathways explaining the conversion of these two intermediate species to pyrene, which consists in a key species in soot formation mechanism.

Acknowledgments

We are indebted to the Centre de Ressources Informatiques (CRI) of the University of Lille and the Centre Régional Informatique et d'Applications Numériques de Normandie (CRIANN) for providing computer time of the theoretical calculations. This work is funded by the CLIMIBIO project. The authors thank the Hauts-de-France region and European Regional Development

Fund for financially support. We appreciated the support from the LABEX CaPPA (Chemical and Physical Properties of the Atmosphere), which is funded by the French National Research Agency (ANR) through the PIA (Programme d'Investissement d'Avenir) under contract ANR-11-LABX-0005-01 and also the Regional Council "Hauts de France" and the "European Funds for Regional Economic Development". This research is funded by Vietnam National Foundation for Science and Technology Development (NAFOSTED) under grant number 103.03-2018.366. The authors thank Dr. Lucia Giarracca for her advice on the kinetic calculations. Our thanks are due to Professor Stephen Klippenstein for providing the MESS program and for his advice and suggestions.

References

[1] A.L. Lafleur, J.P. Longwell, J.A. Marr, P.A. Monchamp, E.F. Plummer, W.G. Thilly, P.P. Mulder, B.B. Boere, J. Cornelisse, J. Lugtenburg, Bacterial and human cell mutagenicity study of some C18H10 cyclopenta-fused polycyclic aromatic hydrocarbons associated with fossil fuels combustion, Envrion. Heal. Perspect. 101 (1993) 146–153.

[2] J. Lewtas, Air pollution combustion emissions: Characterization of causative agents and mechanisms associated with cancer, reproductive, and cardiovascular effects, Mutat. Res. 636 (2007) 95–133.

[3] J.S. Gaffney, N.A. Marley, The impacts of combustion emissions on air quality and climate - From coal to biofuels and beyond, Atmos. Environ. 43 (2009) 23–36.

[4] A.T. Lawal, Polycyclic aromatic hydrocarbons. A review, Cogent Environ. Sci. 3 (2017) 1339841.

[5] F.A. Ahlström, C.U. Ingemar Odenbrand, Combustion characteristics of soot deposits

from diesel engines, Carbon N. Y. 27 (1989) 475–483.

[6] G. Shu, L. Dong, X. Liang, A review of experimental studies on deposits in the combustion chambers of internal combustion engines, Int. J. Engine Res. 13 (2012) 357–369.

[7] H. Richter, J.B. Howard, Formation of polycyclic aromatic hydrocarbons and their growth to soot - A review of chemical reaction pathways, Prog. Energy Combust. Sci. 26 (2000) 565–608.

[8] H. Sabbah, L. Biennier, S.J. Klippenstein, I.R. Sims, B.R. Rowe, Exploring the role of PAHs in the formation of soot: Pyrene dimerization, J. Phys. Chem. Lett. 1 (2010) 2962–2967.

[9] B. Shukla, M. Koshi, Comparative study on the growth mechanisms of PAHs, Combust. Flame. 158 (2011) 369–375.

[10] F. Seitz, A.I.S. Holm, H. Zettergren, H.A.B. Johansson, S. Rosén, H.T. Schmidt, A. Ławicki, J. Rangama, P. Rousseau, M. Capron, R. Maisonny, A. Domaracka, L. Adoui, A. Méry, B. Manil, B.A. Huber, H. Cederquist, Polycyclic aromatic hydrocarbon-isomer fragmentation pathways: Case study for pyrene and fluoranthene molecules and clusters, J. Chem. Phys. 135 (2011).

[11] A. Giordana, A. Maranzana, G. Tonachini, Carbonaceous nanoparticle molcular inception from radical addition and van der Waals coagulation of polycyclic aromatic hydrocarbon-based systems. A theoretical study, J. Phys. Chem. C. 115 (2011) 17237–17251.

[12] M.R. Kholghy, G.A. Kelesidis, S.E. Pratsinis, Reactive polycyclic aromatic hydrocarbon dimerization drives soot nucleation, Phys. Chem. Chem. Phys. 20 (2018) 10926–10938.

[13] J. Hernádez-Rojas, F. Calvo, Coarse-grained modeling of the nucleation of polycyclic aromatic hydrocarbons into soot precursors, Phys. Chem. Chem. Phys. 21 (2019) 5123–

5132.

[14] A.L. Lafleur, J.B. Howard, K. Taghizadeh, E.F. Plummer, L.T. Scott, A. Necula, K.C. Swallow, Identification iof C20H10 dicyclopentapyrenes in flames: Correlation with corannulene and fullerene formation, J. Phys. Chem. 100 (1996) 17421–17428.

[15] M. Frenklach, H. Wang, Detailed modeling of soot particle nucleation and growth, Symp. Combust. 23 (1991) 1559–1566.

[16] A. Raj, M. Sander, V. Janardhanan, M. Kraft, A study on the coagulation of polycyclic aromatic hydrocarbon clusters to determine their collision efficiency, Combust. Flame. 157 (2010) 523–534.

[17] T.S. Totton, A.J. Misquitta, M. Kraft, A quantitative study of the clustering of polycyclic aromatic hydrocarbons at high temperatures, Phys. Chem. Chem. Phys. 14 (2012) 4081–4094.

[18] P. Elvati, A. Violi, Thermodynamics of poly-aromatic hydrocarbon clustering and the effects of substituted aliphatic chains, Proc. Combust. Inst. 34 (2013) 1837–1843.

[19] J.Y.W. Lai, P. Elvati, A. Violi, Stochastic atomistic simulation of polycyclic aromatic hydrocarbon growth in combustion, Phys. Chem. Chem. Phys. 16 (2014) 7969–7979.

[20] Y. Wang, A. Raj, S.H. Chung, Soot modeling of counterflow diffusion flames of ethylene-based binary mixture fuels, Combust. Flame. 162 (2015) 586–596.

[21] M. Frenklach, A.M. Mebel, On the mechanism of soot nucleation, Phys. Chem. Chem. Phys. 22 (2020) 5314–5331.

[22] J.B. Howard, J.P. Longwell, J.A. Marr, C.J. Pope, W.F. Busby Jr., A.L. Lafleur, K. Taghizadeh, Effects of PAH isomerizations on mutagenicity of combustion products, Combust. Flame. 101 (1995) 262–270.

[23] M. Frenklach, D.W. Clary, W.C. Gardiner Jr., S.E. Stein, Detailed kinetic modeling of soot

formation in shock-tube pyrolysis of acetylene, Symp. Combust. 20 (1985) 887–901.

[24] J. Appel, H. Bockhorn, M. Frenklach, Kinetic modeling of soot formation with detailed chemistry and physics: Laminar premixed flames of C2 hydrocarbons, Combust. Flame. 121 (2000) 122–136.

[25] J.A. Miller, C.F. Melius, Kinetic and thermodynamic issues in the formation of aromatic compounds in flames of aliphatic fuels, Combust. Flame. 91 (1992) 21–39.

[26] L. Zhao, R.I. Kaiser, B. Xu, U. Ablikim, M. Ahmed, M.M. Evseev, E.K. Bashkirov, V.N. Azyazov, A.M. Mebel, Low-temperature formation of polycyclic aromatic hydrocarbons in Titan's atmosphere, Nat. Astron. 2 (2018) 973–979.

[27] P. Liu, Y. Zhang, Z. Li, A. Bennett, H. Lin, S.M. Sarathy, W.L. Roberts, Computational study of polycyclic aromatic hydrocarbons growth by vinylacetylene addition, Combust. Flame. 202 (2019) 276–291.

[28] H. Hopf, H. Musso, Preparation of benzene by pyrolysis of cis- and trans-1,3-hexadien-5-yne, Angew. Chem., Int. Ed. Engl. 8 (1969) 680.

[29] R.F.C. Brown, K.J. Harrington, G.L. McMullen, Benzylidenecarbene as a probable intermediate in the interconversion of Ph13C≡CH and PhC≡13CH at 550 oC and 700 oC, J. Chem. Soc., Chem. Comm. (1974) 123–124.

[30] L.T. Scott, M.A. Kirms, M.A. Minton, Thermal rearrangement of aromatic compounds. 2. Isomerization of azulene-3a-13C to Naphthalene-13C, Croat. Chem. Acta. 53 (1980) 643–647.

[31] L.T. Scott, M.A. Kirms, Azulene thermal rearrangements. 13C-labeling studies of automerization and isomerization to naphthalene, J. Am. Chem. Soc. 103 (1981) 5875–5879.

[32] L.T. Scott, Thermal rearrangements of aromatic compounds, Acc. Chem. Res. 15 (1982)

52–58.

[33] L.T. Scott, N.H. Roelofs, Benzene ring contractions at high temperatures. Evidence from the thermal interconversions of aceanthrylene, acephenanthrylene, and fluoranthene, J. Am. Chem. Soc. 109 (1987) 5461–5465.

[34] L.W. Jenneskens, M. Sarobe, Thermal generation and (inter)conversion, Pure Appl. Chem. 68 (1996) 219–224.

[35] M. Sarobe, L.W. Jenneskens, J. Wesseling, U.E. Wiersum, High temperature gas phase syntheses of C20H12cyclopenta-fused polycyclic aromatic hydrocarbons: Benz[l]acephenanthrylene and benz[j]acephenanthrylene and their selective rearrangement to benzo[j]fluoranthene, J. Chem. Soc. Perkin Trans. 2. (1997) 703–708.

[36] M. Sarobe, L.W. Jenneskens, J. Wesseling, J.D. Snoeijer, J.W. Zwikker, U.E. Wiersum, Thermal interconversion of the C16H10 cyclopenta-fused polycyclic aromatic hydrocarbons fluoranthene, acephenanthrylene and aceanthrylyene revisited, Liebigs Ann. (1997) 1207–1213.

[37] M.B. Pastor, A.J. Kuhn, P.T. Nguyen, M. V. Santander, C. Castro, W.L. Karney, Hydrogen shifts and benzene ring contractions in phenylenes, J. Phys. Org. Chem. 26 (2013) 750–754.

[38] I.D. Mackie, R.P. Johnson, Thermal rearrangements of 2-ethynylbiphenyl: a DFT study of competing reaction mechanisms, J. Org. Chem. 74 (2009) 499–503.

[39] J.F. Parent, P. Deslongchamps, High-Temperature Isomerization of Benzenoid Polycyclic Aromatic Hydrocarbons. Analysis through the Bent Bond and Antiperiplanar Hypothesis Orbital Model, J. Org. Chem. 83 (2018) 3299–3304.

[40] P. Desgroux, A. Faccinetto, X. Mercier, T. Mouton, D. Aubagnac Karkar, A. El Bakali, Comparative study of the soot formation process in a “nucleation” and a “sooting” low

pressure premixed methane flame, Combust. Flame. 184 (2017) 153–166..

[41] A. El Bakali, X. Mercier, M. Wartel, F. Acevedo, I. Burns, L. Gasnot, J.-F. Pauwels, P. Desgroux, Modeling of PAHs in low pressure sooting premixed methane flame, Energy. 43 (2012) 73–84.

[42] X. Mercier, O. Carrivain, C. Irimiea, A. Faccinetto, E. Therssen, Dimers of polycyclic aromatic hydrocarbons: the missing pieces in the soot formation process, Phys. Chem. Chem. Phys. 21 (2019) 8282–8294.

[43] M.J. Frisch, G.W. Trucks, H.B. Schlegel, G.E. Scuseria, M.A. Robb, J.R. Cheeseman, G. Scalmani, V. Barone, G.A. Petersson, H. Nakatsuji, X. Li, M. Caricato, A.V. Marenich, J. Bloino, B.G. Janesko, R. Gomperts, B. Mennucci, H.P. Hratchian, J.V. Ortiz, A.F. Izmaylov, J.L. Sonnenberg, D. Williams-Young, F. Ding, F. Lipparini, F. Egidi, J. Goings, B. Peng, A. Petrone, T. Henderson, D. Ranasinghe, V.G. Zakrzewski, J. Gao, N. Rega, G. Zheng, W. Liang, M. Hada, M. Ehara, K. Toyota, R. Fukuda, J. Hasegawa, M. Ishida, T. Nakajima, Y. Honda, O. Kitao, H. Nakai, T. Vreven, K. Throssell, J.A. Montgomery Jr, J.E. Peralta, F. Ogliaro, M.J. Bearpark, J.J. Heyd, E.N. Brothers, K.N. Kudin, V.N. Staroverov, T.A. Keith, R. Kobayashi, J. Normand, K. Raghavachari, A.P. Rendell, J.C. Burant, S.S. Iyengar, J. Tomasi, M. Cossi, J.M. Millam, M. Klene, C. Adamo, R. Cammi, J.W. Ochterski, R.L. Martin, K. Morokuma, O. Farkas, J.B. Foresman, D.J. Fox, Gaussion 16 Rev. A.03, (2016).

[44] A.D. Becke, Density-functional thermochemistry. III. The role of exact exchange, J. Chem. Phys. 98 (1993) 5648.

[45] P.J. Stephens, F.J. Devlin, C.F. Chabalowski, M.J. Frisch, Ab Initio Calculation of Vibrational Absorption and Circular Dichroism Spectra Using Density Functional Force Fields, J. Phys. Chem. 98 (1994) 11623–11627.

[46] Y. Zhao, D.G. Truhlar, The M06 suite of density functionals for main group thermochemistry, thermochemical kinetics, noncovalent interactions, excited states, and transition elements: Two new functionals and systematic testing of four M06-class functionals and 12 other function, Theor. Chem. Acc. 120 (2008) 215–241.

[47] A.D. Boese, J.M.L. Martin, Development of density functionals for thermochemical kinetics, J. Chem. Phys. 121 (2004) 3405–3416.

[48] S. Grimme, S. Ehrlich, L. Goerigk, Effect of the damping function in dispersion corrected density functional theory, J. Comput. Chem. 32 (2011) 1456–1465.

[49] S. Grimme, J. Antony, S. Ehrlich, H. Krieg, A consistent and accurate ab initio parametrization of density functional dispersion correction (DFT-D) for the 94 elements H-Pu, J. Chem. Phys. 132 (2010) 154104.

[50] J.A. Montgomery, M.J. Frisch, J.W. Ochterski, G.A. Petersson, A complete basis set model chemistry. VII. Use of the minimum population localization method, J. Chem. Phys. 112 (2000) 6532–6542.

[51] M. Martínez González, F.G.D. Xavier, J. Li, L.A. Montero-Cabrera, J.M. Garcia de la Vega, A.J.C. Varandas, Role of Augmented Basis Sets and Quest for ab Initio Performance/Cost Alternative to Kohn–Sham Density Functional Theory, J. Phys. Chem. A. 124 (2020) 126–134.

[52] A.J.C. Varandas, CBS extrapolation in electronic structure pushed to the end: a revival of minimal and sub-minimal basis sets, Phys. Chem. Chem. Phys. 20 (2018) 22084–22098..

[53] A.J.C. Varandas, M. Martínez González, L.A. Montero-Cabrera, J.M. Garcia de la Vega, Assessing How Correlated Molecular Orbital Calculations Can Perform versus Kohn–Sham DFT: Barrier Heights/Isomerizations, Chem. – A Eur. J. 23 (2017) 9122–9129.

[54] A.J.C. Varandas, Straightening the Hierarchical Staircase for Basis Set Extrapolations: A

Low-Cost Approach to High-Accuracy Computational Chemistry, Annu. Rev. Phys. Chem. 69 (2018) 177–203.

[55] A. Galano, J.R. Alvarez-Idaboy, A computational methodology for accurate predictions of rate constants in solution: Application to the assessment of primary antioxidant activity, J. Comput. Chem. 34 (2013) 2430–2445.

[56] A. Galano, J.R. Alvarez-Idaboy, Kinetics of radical-molecule reactions in aqueous solution: A benchmark study of the performace of density functional methods, J. Comput. Chem. 35 (2014) 2019–2026.

[57] D.Q. Dao, T.C. Ngo, M.T. Nguyen, C.N. Pham, Is vitamin A an antioxidant or a pro-oxidant?, J. Phys. Chem. B. 121 (2017) 9348–9357.

[58] K.K. Irikura, Thermo. PL, (2002).

[59] L. Deng, T. Ziegler, The determination of intrinsic reaction coordinates by density functional theory, Int. J. Quantum Chem. 52 (1994) 731–765.

[60] R. Seeger, J.A. Pople, Self-consistent molecular orbital methods. XVIII. Constraints and stability in Hartree–Fock theory, J. Chem. Phys. 66 (1977) 3045–3050.

[61] R. Bauernschmitt, R. Ahlrichs, Stability analysis for solutions of the closed shell Kohn–Sham equation, J. Chem. Phys. 104 (1996) 9047–9052.

[62] Y. Georgievskii, S.J. Klippenstein, MESS.2016.3.23, (2016).

[63] Y. Georgievskii, J.A. Miller, M.P. Burke, S.J. Klippenstein, Reformulation and Solution of the Master Equation for Multiple-Well Chemical Reactions, J. Phys. Chem. A. 117 (2013) 12146–12154.

[64] H. Wang, M. Frenklach, A detailed kinetic modeling study of aromatics formation in laminar premixed acetylene and ethylene flames, Combust. Flame. 110 (1997) 173–22

[65] J.A. White, Lennard-Jones as a model for argon and test of extended renormalization

group calculations, J. Chem. Phys. 111 (1999) 9352–9356.

[66] X. Mercier, A. Faccinetto, S. Batut, G. Vanhove, D.K. Božanić, H.R. Hróðmarsson, G.A. Garcia, L. Nahon, Selective identification of cyclopentaring-fused PAHs and side-substituted PAHs in a low pressure premixed sooting flame by photoelectron photoion coincidence spectroscopy, Phys. Chem. Chem. Phys. 22 (2020) 15926–15944.

[67] T. Mitra, C. Chu, A. Naseri, M.J. Thomson, Polycyclic aromatic hydrocarbon formation in a flame of the alkylated aromatic trimethylbenzene compared to those of the alkane dodecane, Combust. Flame. 223 (2021) 495–510.

[68] A.C. Hazell, F.K. Larsen, M.S. Lehmann, A neutron diffraction study of the crystal structure of pyrene, C16H10, Acta Crystallogr. B. 28 (1972) 2977–2984.

[69] J.V. Goodpaster, J.F. Harrison, V.L. McGuffin, Ab initio study of polycyclic aromatic hydrocarbons in their ground and excited states, J. Phys. Chem. A. 102 (1998) 3372–3381.

[70] S. Sinha, R.K. Rahman, A. Raj, On the role of resonantly stabilized radicals in polycyclic aromatic hydrocarbon (PAH) formation: Pyrene and fluoranthene formation from benzyl-indenyl addition, Phys. Chem. Chem. Phys. 19 (2017) 19262–19278.

[71] D. Wang, A. Violi, D.H. Kim, J.A. Mullholland, Formation of naphthalene, indene, and benzene from cyclopentadiene pyrolysis: A DFT study, J. Phys. Chem. A. 110 (2006) 4719–4725.

[72] O.V. Dorofeeva, Thermodynamic properties of gaseous polycyclic aromatic hydrocarbons containing five-membered rings, Moscow, 1989.

[73] C.J. Pope, Thermochemical properties of curved PAH and fullerenes: A group additivity method compared with MM3(92) and MOPAC predictions, J. Phys. Chem. 99 (1995) 4306–4316.

[74] J. Yu, R. Sumathi, W.H. Green Jr., Accurate and efficient method for predicting

thermochemistry of polycyclic aromatic hydrocarbons - Bond-centered group additivity, J. Am. Chem. Soc. 126 (2004) 12685–12700.

[75] G. Blanquart, H. Pitsch, Thermochemical properties of Polycyclic Aromatic Hydrocarbons (PAH) from G3MP2B3 calculations, J. Phys. Chem. A. 111 (2007) 6510–6520.

[76] G. Blanquart, H. Pitsch, Thermochemical properties of polycyclic aromatic hydrocarbons (PAH) from G3MP2B3 calculations, J. Phys. Chem. A. 111 (2007) 6510–6520.

[77] T.C. Allison, D.R. Burgess Jr., First-principles prediction of enthalpies of formation for polycyclic aromatic hydrocarbons and derivatives, J. Phys. Chem. A. 119 (2015) 11329–11365.

[78] S. Rayne, K. Forest, A G4MP2 theoretical study on the gas phase enthalpies of formation for various polycyclic aromatic hydrocarbons (PAHs) and other C10 through C20 unsaturated hydrocarbons, in: Nat. Procedings, 2011.

[79] D. Khiri, D.Q. Dao, B.T. Nguyen, L. Gasnot, F. Louis, A. El Bakali, Theoretical Investigation of the Reaction of Pyrene Formation from Fluoranthene, J. Phys. Chem. A. 123 (2019) 7491–7498.

[80] R. Whitesides, D. Domin, R. Salomón-Ferrer, Lester William A., M. Frenklach, Graphene Layer Growth Chemistry: Five- and Six-Member Ring Flip Reaction, J. Phys. Chem. A. 112 (2008) 2125–2130.

[81] M. Frenklach, Reaction mechanism of soot formation in flames, Phys. Chem. Chem. Phys. 4 (2002) 2028–2037.

« Étranger tu me demandes quel est mon père ? Je te répondrai sans détour. Ma mère m'a dit que j'étais le fils d'Ulysse. Pour moi, je n'en sais rien car nul ne connait son père ».

Le temps a fait son œuvre. ***1***

1 Introduction

Johannes Reil a introduit le terme de « psychiatrie » il y a plus de 200 ans [1]. Il soutenait que la psychiatrie devait démontrer que les troubles mentaux ne sont pas des défaillances morales, mais des maladies semblables à d'autres atteintes physiques. Il fallait donc créer une discipline médicale prouvant que les maladies organiques et psychiques étaient toutes deux des sujets légitimes de la médecine. Pour cela, il fallait passer par la recherche des origines des troubles mentaux. La psychiatrie n'est donc historiquement pas exempte de cette quête des origines. Elle doit cependant s'accommoder d'une multiplicité de systèmes de valeurs. Il y a quelques années, les débats épistémologiques et théoriques de la psychiatrie portaient sur le caractère organique ou psychogène de la pathologie mentale. Le débat actuel portant sur l'explication des troubles mentaux s'est tourné vers la question de l'intrication du génotype au phénotype psychiatrique [2]. Une conception réductionniste décrit la génétique comme la condition d'existence des niveaux d'explications supérieurs du vivant, qu'ils soient moléculaires, cellulaires, de connectivité, physiologiques ou comportementaux [3]. Cette condition de possibilité, si elle peut certes être critiquée, nécessite cependant que la psychiatrie s'intéresse mieux à la génétique, afin d'en comprendre les implications et les limites [4]. Le but de cet article est de proposer un cadre de travail interdisciplinaire favorisant la communication entre ces deux disciplines médicales.

1 Conseillé par le relecteur numéro trois, 2020,citant le *Précis de psychiatrie*, Leviy-Valensi, 1926, citant le *Télémaque* de Fénelon, 1699.

2 Méthodes

Dans un premier temps, nous présentons les bases de la génétique. Pour cela, nous mettons en avant la manière dont le séquençage génétique de nouvelle génération est exploité en santé mentale. Dans un second temps, nous analysons l'application pratique du Plan France Médecine Génomique 2025 [5] à la psychiatrie. Enfin, nous présentons trois possibilités fournies par la génétique à la psychiatrie : celle d'un diagnostic causal, celle d'un conseil génétique et celle d'une psychiatrie de précision. Nous analysons les limites de la génétique en psychiatrie, à travers l'interprétation des données génétiques et à travers la difficulté d'associer une étiologie génétique à une prise en charge spécifique.

3 Résultats

3.1 Définitions : gène, variant et séquençage à haut débit

Comme l'écrivaient Riley et Kendler, les gènes sont « des parties dynamiques de systèmes biologiques d'une immense complexité » [6]. Ils sont habituellement décrits comme les unités d'ADN contrôlant l'héritage phénotypique, selon la génétique mendélienne ou médicale [7], mais peuvent encore être conçus de différentes manières selon que l'on se place du point de vue de l'épidémiologie génétique [8] ou de la génétique moléculaire [9].

Le polymorphisme génétique renvoie à l'existence de variants non pathologiques sur une même séquence ou un même nucléotide (la plus petite portion de l'ADN). À titre d'exemple, deux individus possèdent environ cinq millions de différences dans leur ADN. Ces différences, nommées variants, expliquent les spécificités des phénotypes individuels. On considère qu'un variant est témoin du polymorphisme de l'ADN lorsqu'il diffère chez plus d'1 % de la population. Un variant

correspond donc à une séquence d'ADN présentant une variation d'un ou plusieurs nucléotides et qui peut être regroupé sur un ou plusieurs gènes. La notion de variant permet de mieux comprendre la génétique contemporaine, car le seul concept de gène ne suffit plus à expliquer la clinique psychiatrique. Les variants peuvent être des bases isolées sur l'ADN (SNP pour *Single Nucleotid Polymorphism*, par exemple la substitution d'une base, détectés par séquençage), des séquences entières (CNP pour *Copy Number Polymorphism*, détectées par analyse chromosomique sur puce à ADN) ou des échanges entre séquences (BSV pour *Balanced Structural Variant*, ou translocation, qui peut être équilibrée ou non). Les variants sont classés de manière systématique. Cette classification, résumée par les critères de l'*American College of Medical Genetics* (ACMG, [10]), est essentielle à la compréhension de la génétique contemporaine. Ainsi, lorsqu'un biologiste cible un variant génétique particulier, il peut l'affecter dans une des cinq classes en s'aidant de bases de données. Il peut alors le considérer comme bénin (Classe 1) ; probablement bénin ; VOUS (*Variant Of Uncertain Signifiance*) (Classe 2), critère qui renvoie à un variant non encore connu ou pour lequel on ne peut pas établir de pathogénicité ; probablement pathologique (Classe 3) ; pathologique (Classe 4). À ces cinq classes s'ajoutent des variants de susceptibilité, qui sont des variants nécessaires au développement d'une pathologie sans pour autant être suffisants pour l'expliquer entièrement.

D'un point de vue technique, deux types d'examens utilisant le « séquençage de nouvelle génération », ou séquençage à haut débit, permettent d'explorer des ensembles de gènes et de variants qui témoigneraient de la survenue de troubles psychiatriques [11]. Premièrement, les panels de gènes sont des ensembles de gènes (de 10 à plus de 300) dont l'implication dans un trouble a déjà été démontrée. Par exemple, le panel DI (pour déficience intellectuelle) comprend un ensemble de gènes connus pour être fréquemment responsables de déficience intellectuelle. Les panels sont donc utilisés pour rechercher un ensemble de gènes correspondant à un trouble ou à un syndrome. Ce genre de panel est en cours de développement en psychiatrie clinique en France. Une deuxième technique fournie par la génétique à la psychiatrie correspond à l'analyse de l'exome, qui étudie la

partie codante du génome (les exons représentent environ 1,5 % du génome), c'est-à-dire les segments des gènes transcrits en ARN (Acide RiboNucléique) messagers qui seront codés en protéines. Le séquençage de l'exome est actuellement disponible en psychiatrie dans le cadre de la recherche clinique. Cette technique d'exploration génomique fournit des signatures moléculaires et renseigne sur les endophénotypes des troubles psychiatriques [12].

Au sein de la génétique, de nombreux niveaux de complexité sont intégrés : des interactions gène-gène (épistasie), des interactions gène-environnement, des fonctions différentes pour un même gène (pléïotropie et *gene sharing*), etc [13]. Au sein de la psychiatrie, les troubles sont dits multifactoriels (ou complexes), car leur physiopathologie implique l'action conjointe de plusieurs gènes et/ou de nombreux facteurs environnementaux. Au premier abord, il semble donc difficile de comprendre quelles sont les contributions de la génétique à la psychiatrie. Cependant, ces dernières années l'interaction entre génétique et psychiatrire ne cesse d'augmenter [14]. Nous allons donc en présenter les implications sur les plans clinique, thérapeutique, expérientiel et de santé publique.

3.2 Génétique et psychiatrie

Les informations apportées par la génétique à la psychiatrie possèdent une pertinence clinique, un rôle thérapeutique, un effet psychologique et des retentissements sur la santé publique.

Sur le plan clinique, la génétique oriente le diagnostic et le pronostic. Par exemple, la survenue d'une psychose est statistiquement plus élevée en présence d'une microdélétion 22q11.2 [15]. Si le clinicien émet une hésitation quant au diagnostic, la décision clinique est alors renforcée par l'apport de la génétique.

Sur le plan thérapeutique, la génétique permet de fournir un traitement de précision. Le syndrome de Smith-Magenis, lié à une microdélétion en 17p11.2 emportant le gène *RAI1* (ou à une mutation de ce même gène) entraîne, entre autres, des troubles du sommeil. Il a été démontré que dans ce syndrome, un traitement par mélatonine, hormone naturelle de l'endormissement, était plus efficace

et mieux toléré qu'un autre hypnotique médicamenteux [16]. La génétique ouvre ainsi le champ de l'amélioration des indications thérapeutiques. Il ne s'agit pas tant des thérapies géniques que de la possibilité d'une médecine de précision. La médecine de précision repose sur une stratification du risque pour un ensemble de patients. Elle cherche à établir des strates formées de sous-groupes de malades. Par exemple, la pharmacogénomique psychiatrique permet de confirmer la cinétique et la dynamique des médicaments en fonction du polymorphisme génétique [17].

Sur le plan expérientiel, la reconnaissance d'une anomalie génétique apporte un certain réconfort face à l'adversité de la maladie psychiatrique [18]. La possibilité de labelliser le trouble psychiatrique, c'est-à-dire en donner une explication, a un impact considérable sur le vécu expérientiel du patient et de son entourage. Les retours d'expérience de la part des soignants sont également favorables [19].

Enfin, sur le plan de la santé publique, la génétique permet une réduction de l'errance diagnostique, une diminution du nombre de bilans diagnostiques et des bénéfices liés à la réduction des coûts thérapeutiques. Ensuite, le conseil génétique offre des pistes prometteuses pour la psychiatrie.

La pertinence de la génétique en psychiatrie est certaine. Mais en pratique, afin de mieux comprendre son ancrage en santé mentale, nous proposons d'explorer les différents enjeux scientifiques, cliniques, technologiques, économiques ou de santé publique qui sont décrits dans le plan France Médecine Génomique 2025.

3.3 Le Plan France Médecine Génomique 2025 : son application en psychiatrie

Le Plan France Médecine Génomique 2025 (PFMG2025) a été adressé par le Premier ministre à l'Alliance pour la Vie et la Santé (Aviesan), en avril 2015, afin d'accélérer la mise en place du diagnostic génétique en France. Il propose l'étude de génomes entiers, et non pas l'étude de panels ou d'exomes. Le PFMG2025 prévoit de prendre en charge 235 000 séquençages de génomes par an, tout en veillant à prendre en compte l'avis des usagers, des associations de malades et de la société

en général. Il s'appuie sur quatre projets pilotes : le cancer avec le projet « Multipli », les maladies rares avec le projet « Defidiag » qui concerne les patients ayant une déficience intellectuelle, les maladies communes avec le projet « Glucogen » pour le diabète et des études en population générale avec le projet « Popgen ». Le Plan se déploie autour de quatre enjeux, et l'enjeu éthique est prépondérant dans chacun d'eux :

1. Un enjeu de santé publique : la médecine génomique réorganise l'organisation de la santé publique par la modification des parcours de soin de ses bénéficiaires. Par exemple, un nombre important de patients pourront prochainement bénéficier d'un génome en routine.
2. Un enjeu scientifique et clinique : l'approche génomique explore à la fois le niveau moléculaire des pathologies tout en apportant des bénéfices thérapeutiques au patient. Grâce à cette exploration fournissant des biomarqueurs génétiques mêlés à des données cliniques et environnementales, de mutiples bases de données génétiques sont en cours de constitution.
3. Un enjeu technologique : les sciences et technologies de l'information et la communication convergent actuellement vers les sciences de la vie et de la santé. Les acteurs traditionnels de la santé, du médicament, de l'imagerie ou des équipements scientifiques travaillent avec les industriels des technologies de l'information, du big data, des objets connectés et de la médecine connectée.
4. Un enjeu économique : le plan entraîne une redistribution des coûts au sein du système de soin, avec le développement de nouvelles filières stratégiques, médicales et scientifiques, notamment dans le but d'éviter une dépendance technologique vis-à-vis des autres pays engagés dans cette démarche.
5. Les impératifs éthique s'appliquent à ces quatre enjeux. Ils portent sur le consentement, l'accès, l'utilisation de données et leur anonymisation vis-à-vis des tiers. Ils interrogent la gestion des découvertes additionnelles (découvertes non prévues lors de la recherche génétique intiale, qui peuvent être secondaires ou incidentes). Ils prennent en compte le risque d'exclusion des

personnes n'ayant pas accès à de telles analyses. Ainsi, sans qu'il ne les cite explicitement, le PFMG2025 respecte trois principes éthiques clés : le principe d'autonomie (« Vous êtes libres de disposer de toutes les informations vous concernant. »), le principe de bienfaisance (« La médecine prend soin de ne vouloir que le meilleur pour vous. ») et le principe d'équité (« Un accès au soin équitable pour tous. ») [20].

Actuellement, le PFMG2025 s'est concrétisé par :

- La mise en place de deux platefromes pilotes : SeqOIA pour la moitié nord de la France et AURAGEN pour le moitié Sud et les départements d'Outre-mer ;
- La publication de 14 préindications pour des patients atteints de maladies rares ou de cancers ;
- La mise en place par les filières de soins maladies et les réseaux INCA d'un parcours génomique [21].

4 Discussion

Les enjeux du PFMG2025 se répercutent à plusieurs niveaux en psychiatrie. Le diagnostic psychiatrique mêle les données cliniques classiques aux données génomiques individualisées. Cela offre une expertise multidisciplinaire conforme aux données actuelles de la science. Les capacités de dialogue avec les autres spécialités se renforcent. L'offre éducative se complexifie, par exemple au travers du réseau des associations de malades qui se saisissent de cette individualisation du soin et cherchent à comprendre les outils de cette psychiatrie personnalisée pour mieux s'impliquer, de manière participative, dans la trajectoire médicale qui leur est proposée. Ensuite, le PFMG2025 intègre une perspective de précision dans la psychiatrie. Cette perspective permet de valider de nouvelles indications thérapeutiques dans un grand nombre de troubles mentaux, notamment grâce à la stratification des patients. Par exemple, des diagnostics psychiatriques ambigüs peuvent être